RMetS
Royal Meteorological Society

Effects of optical depth variability on contrail radiative forcing

Bernd Kärcher*and Ulrike Burkhardt

Deutsches Zentrum für Luft- und Raumfahrt, Institut für Physik der Atmosphäre, Oberpfaffenhofen, Germany

*Correspondence to: B. Kärcher, Deutsches Zentrum für Luft- und Raumfahrt, Oberpfaffenhofen, Wessling D-82234, Germany. E-mail: bernd.kaercher@dlr.de

Line-shaped contrails arising from aircraft emissions affect radiative forcing. The magnitude of the radiative forcing from contrails depends strongly on their optical depth and their spatial and temporal variability caused by dynamical and microphysical processes. Here we investigate the significance of this variability, both for modelling contrail radiative forcing and estimating thresholds for the detection of contrails in satellite imagery. Ignoring the variability of contrail optical depth in models by prescribing a mean optical depth may overestimate mean net radiative forcing by 10−20%. Undersampling of optically thin line-shaped contrails by passive satellite remote sensing is linked to the inability to detect flux changes in the outgoing long-wave radiation below $\approx 3\,\mathrm{W\,m^{-2}}$ for conditions over the eastern North Pacific. Consideration of these findings aids efforts to better quantify uncertainties in aviation climate assessments.

Key Words: aviation; aircraft emissions; contrails; radiative forcing; optical depth

Received 25 April 2012; Revised 16 August 2012; Accepted 12 September 2012; Published online in Wiley Online Library 12 November 2012

Citation: Kärcher B, Burkhardt U. 2013. Effects of optical depth variability on contrail radiative forcing. *Q. J. R. Meteorol. Soc.* **139**: 1658–1664. DOI:10.1002/qj.2053

1. Introduction

Line-shaped contrails formed by cruising jet aircraft persist in air that is supersaturated with respect to ice and spread into cirrus-like clouds (Fahey and Schumann, 1999). We refer to contrail cirrus as contrails of all ages and shapes, including line-shaped contrails. Contrail cirrus coverage varies both spatially and temporally, mainly dependent on the synoptic situation (Burkhardt and Kärcher, 2009). The global radiative forcing of contrail cirrus, including an offsetting component arising from the reduction of natural cirrus, was found to exceed that of previously accumulated aircraft carbon dioxide emissions, making contrail cirrus the single largest radiative forcing (RF) component associated with aviation (Burkhardt and Kärcher, 2011). The RF of contrail cirrus was also found to be much larger than that of line-shaped contrails only. Observational datasets of contrail cirrus are not available. Consequently, the need for studies characterizing line-shaped contrails remains, as only those can be relatively easily identified in observations and can therefore be used to validate models. Measurements of contrail properties are sparse and suffer from a number of uncertainties (Heymsfield *et al.*, 2010).

Contrail optical depth exhibits large variability (Kärcher *et al.*, 2009, hereafter referred to as K09). The importance of correctly representing optical depth variability for estimates of line-shaped contrail cloud radiative forcing (CRF) has been discussed in an earlier study (Kärcher *et al.*, 2010). Several global contrail RF estimates exist, based on global climate models (GCMs) or on radiative transfer models (RTMs). Estimates from RTMs using prescribed contrail parameters (including spatial coverage) depend strongly on the assumed contrail optical depth.

Here, we address two sources of contrail optical depth variability, the first arising from the variations of the dynamical forcings (meteorological conditions), and the second arising from the heterogeneity of microphysical properties. Both sources contain spatial and temporal components and may cause a bias in calculated CRF (variability bias). RTMs with a prescribed mean optical depth do not represent these types of variability at

all, while GCMs cover some portion of both sources of variability, depending on the model's spatial and temporal resolution and the microphysical representation of contrails.

We have emphasized the importance of using consistent datasets of contrail coverage and optical depth in order to infer global contrail RF and investigated the detectability of optically thin contrails in satellite observations (K09; Kärcher *et al.*, 2010). In this study, we explore the consequences of optical depth variability for CRF both with respect to model simulations (addressing the variability bias) and satellite observations (addressing CRF detection thresholds). We use a microphysical cloud model, driven by prescribed variability in the cloud-controlling factors, to simulate many single persistent contrails evolving in a wide range of atmospheric conditions. Studies using satellite observations did not specify the ages of detectable contrails. Therefore, we assume that the relatively young contrails simulated with our model (ages $\leq$4 h) are comparable to the line-shaped contrails detectable in satellite imagery. All CRF values reported here have been calculated assuming full coverage. They need to be combined with actual coverages of persistent contrails to infer regional or global contrail RF.

2. Methodology

We calculate the instantaneous CRF, defined as the changes in radiative fluxes due to contrails, by combining the contrail simulations with a parametrized radiative transfer scheme. We set up a framework to calculate the broadband flux changes in the short-wave (SW) and long-wave (LW) spectral region. The combination of a radiation scheme with a cloud model that provides statistics of many individual contrail microphysical properties makes it mandatory that such a scheme should be simple, yet capturing the relevant physical mechanisms affecting CRF.

2.1. Radiative transfer parametrization

The SW CRF resulting from the insertion of a homogeneous contrail layer in a plane-parallel atmosphere is expressed as

$$\Delta F_{\mathrm{SW}}=-\overline{F}\Delta\mathcal{A},$$

where $\Delta\mathcal{A}$ is the enhancement in planetary albedo inducing a cooling tendency. The global mean downwelling SW radiative flux

$$\overline{F}=F_{\odot}\frac{(1-C)}{4}$$

is given by the solar constant $F_{\odot}$=1370 W m^{-2} and the average natural cloud fraction C=0.6 (Charlson *et al.*, 1992). Monodirectional solar radiation is incident at a zenith angle θ. Allowing the atmosphere and surface below the layer to be reflective with an effective albedo A, we apply a two-stream approach leading to

$$\Delta\mathcal{A}=r-A\left[1-\frac{(1-r)^2}{1-rA}\right]$$

(Twomey, 1977), with the cloud reflectance

$$r=\left(\frac{\beta\tau}{\mu}\right)\frac{1}{1+\beta\tau/\mu}$$

(Coakley and Chylek, 1975), the upscattered fraction of incident sunlight, β, the SW cloud optical depth, τ, and $\mu=\cos\theta$. According to aircraft observations (Febvre *et al.*, 2009), asymmetry factors of contrails are g=0.827 and g=0.787 for contrail ages of 2.5 min and 20 min, respectively. Values for older contrails have not been measured, but cirrus clouds probed in a similar environment showed $g=0.79$. We use a fixed value, $g=0.8$, to calculate

$$\beta=0.5-\frac{0.75\mu g}{1+g}$$

(Rockel *et al.*, 1991) for contrails up to 4 h old. Varying g in the range 0.75−0.85 bounding the observations introduces an uncertainty in β of $\pm$5% in our model for θ=30°.

The LW CRF is the difference, ΔF_{LW}, between the global mean outgoing flux without (F_{b}) and with (F_{c}) a contrail layer at temperature T_{c}, i.e. $\Delta F_{\mathrm{LW}}=F_{\mathrm{b}}-F_{\mathrm{c}}$. F_{b} is given by σT_{b}^4, with the Stefan–Boltzmann constant σ and the background brightness temperature T_{b} (characterizing the radiation flux without contrails). To calculate F_{c}, we include the emissivity $E=1-\exp(-0.468\,\tau^{0.988})$ (Liou *et al.*, 1990), since contrails do not act as perfect black bodies. The contrail layer reduces the outgoing LW flux in proportion to E,

$$F_{\mathrm{c}}=\sigma\left\{ET_{\mathrm{c}}^4+(1-E)T_{\mathrm{b}}^4\right\}.$$

This results in $\Delta F_{\mathrm{LW}}=\sigma E(T_{\mathrm{b}}^4-T_{\mathrm{c}}^4)$, a warming tendency that increases with decreasing contrail temperature.

As detailed in the appendix, our parametrization correctly predicts the principal behaviour of CRF(τ) for contrail regions with optical depth between $\tau<0.3$ (optically thin) and $\tau>1$ (optically thick). All CRF values reported here use fixed values A=0.3 and θ=30°, and selected values for T_{b}. The net CRF is given by $\Delta F=\Delta F_{\mathrm{SW}}+\Delta F_{\mathrm{LW}}$ in units of W m^{-2}. In principle, it is possible to define CRF in other units. Here, we adopt the common convention as used for natural clouds since this enables a direct comparison with results from other studies.

2.2. Contrail simulations

The optical depth information used in the computation of CRF is supplied by the cloud model, which calculates the approximate evolution of contrails in 2D geometry accounting for ice particle depositional growth, sedimentation, and wind-shear-induced spreading in ice-supersaturated layers of variable thicknesses (K09). The probability distribution function (PDF) shapes were constrained by observations and simulations. The simulated young contrails all evolve in ice supersaturated air for up to 4 h; actual lifetimes can be shorter, e.g. when most ice crystals rapidly sediment through very shallow but strongly supersaturated layers.

In the model, PDFs of temperature, relative humidity over ice (RHI), vertical shear of the horizontal wind, and ice-supersaturated layer depth are prescribed, representing the spatial and temporal variability of these controlling factors. The model was applied with varying combinations of those parameters drawn from the respective PDFs. Mean values and spreads of these PDFs were constrained using data from weather analyses and observations. Optical depths and CRFs were calculated by column-wise integration of the SW extinction efficiency over the simulated ice particle size distributions. Since the contrail model

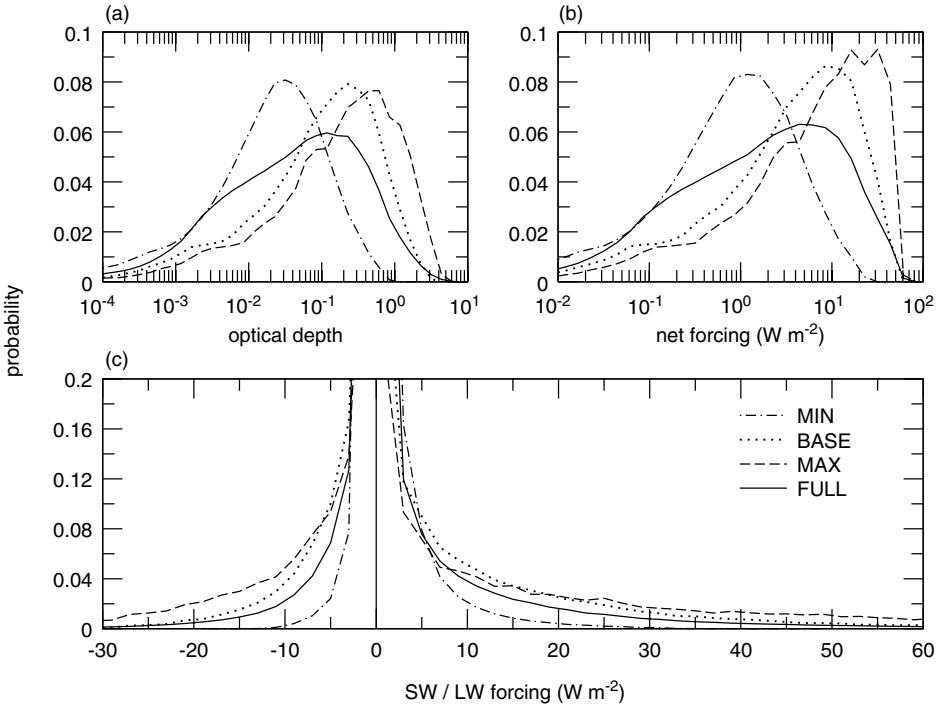

Figure 1. Normalized probability distribution functions of (a) optical depth, (b) net radiative flux change and (c) its short-wave ($\leq$0) and long-wave ($\geq$0) contributions for midlatitude contrails (age <4 h) at 230 hPa pressure altitude. Cases assume variability in temperature (Gaussian), vertical wind shear (Weibull), vertical extent of ice supersaturated layers (double Weibull), and a mean relative humidity over ice (without variability). Mean values are 0.004 s^{-1}, 1 km, and 115% (BASE), respectively, the latter two changed to 0.002 s^{-1} and 125% (MAX) and 0.008 s^{-1} and 105% (MIN). Case FULL is identical to BASE, but assumes exponential variability in RHI using the same mean value. Mean temperature and standard deviation is 218$\pm$2 K, and background brightness temperature is 255 K in all cases.

Table 1. Calculated short-wave, long-wave, and net young contrail radiative forcing (W m^{-2}). Instantaneous radiative forcings correspond to 100% contrail coverage and were averaged over the probability distributions of optical depth (pdf) simulated by the cloud model, or were evaluated at the corresponding mean optical depths (mod). Mean optical depth, variance, and dispersion of PDF(τ) are denoted by τ_m, σ_τ^2, and δ_τ, respectively. Relative differences, Δ, defined as ('pdf'-'mod')/'pdf', are rounded values. Case PAC refers to the Pacific case study discussed in section 3.2.

	τ_m	σ_τ^2	δ_τ	$\overline{\Delta F}_{SW}$			$\overline{\Delta F}_{LW}$			$\overline{\Delta F}$		
				pdf	mod	Δ (%)	pdf	mod	Δ (%)	pdf	mod	Δ (%)
MIN	0.05	0.008	1.8	−0.87	−0.89	−2	2.82	2.94	−4	1.95	2.05	−5
BASE	0.26	0.144	1.5	−3.83	−4.14	−8	11.70	13.20	−13	7.87	9.06	−15
MAX	0.50	0.476	1.4	−6.71	−7.57	−13	19.70	23.50	−19	12.99	15.93	−23
FULL	0.20	0.160	2.0	−2.78	−3.10	−12	8.74	9.96	−14	5.96	6.86	−15
PAC	0.15	0.137	2.5	—	—	—	12.10	14.60	−21	—	—	—

assumes one combination of dynamical forcings in each contrail simulation–equivalent to a constant atmospheric environment in which the contrails evolve–the associated microphysical variability is a conservative estimate. We generated model statistics by carrying out some ten thousand young contrail simulations.

3. Results and discussion

3.1. Contrail optical depth and radiative forcing statistics

We first investigate the error in CRF introduced by the assumption of a constant contrail optical depth. Model statistics of τ and RF for line-shaped contrails are provided in Figure 1. We study two average cases, BASE (assuming a δ-function for RHI) and FULL (exponential PDF for RHI with the same mean value as in BASE). We vary PDF (RHI) because PDF (τ) is sensitive to this choice. We also vary the mean RHI and mean shear values (see Figure 1 caption) relative to BASE to cover more (MAX) or less (MIN) favourable conditions for contrail development, but use a fixed background brightness temperature. The cases MIN, MAX, BASE and FULL do not represent any specific region or observation case. Rather we defined them to discuss the general dependencies of the PDF properties on various assumptions regarding the cloud-controlling factors.

The optical depths cover a wide range of values including a substantial number of subvisible data points with τ <0.02, i.e. values smaller than the approximate visibility limit (Figure 1(a)). The fractions of subvisible contrails are: 55% (MIN), 25% (BASE), 20% (MAX), and 40% (FULL). All PDFs have large variances, σ_τ^2, and are highly skewed towards small optical depth values. The mean optical depths, τ_m, given in Table 1, increase with increasing supersaturation and decreasing wind shear (MIN$\rightarrow$BASE$\rightarrow$MAX), as more water vapour deposits on the ice crystals and each cloud column contains more cloud ice. The exponential PDF (RHI) in case FULL is largest at low supersaturations and results in a variance of PDF (τ) comparable to that of case BASE, favouring optically thin contrails. All cases, except

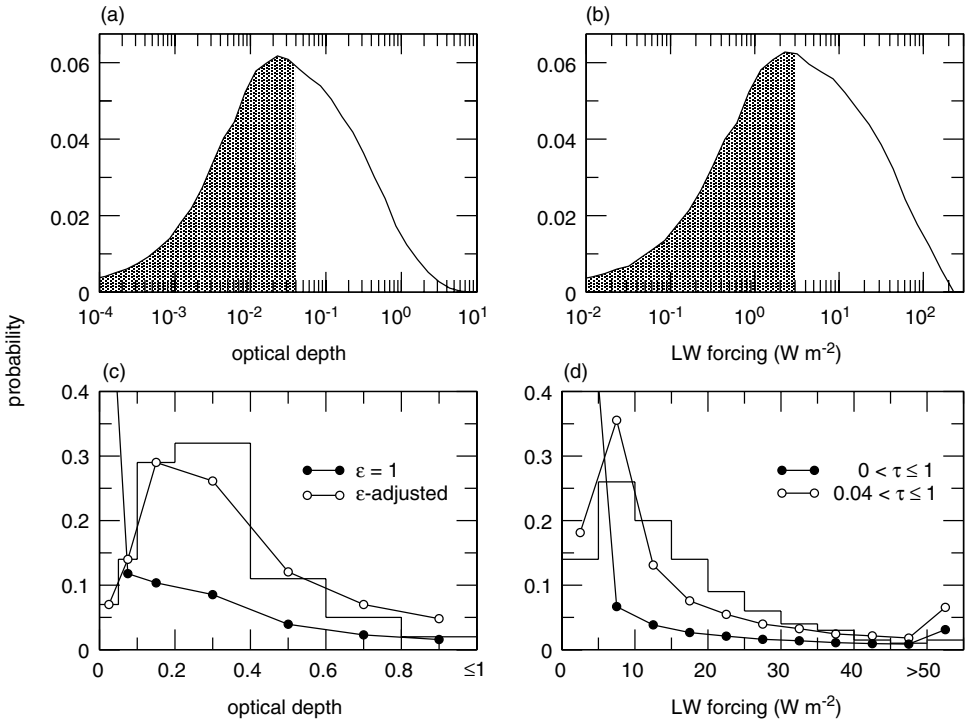

Figure 2. Normalized probability distributions of (a, c) optical depth and (b, d) long-wave radiative flux change. Curves without symbols (all) and with filled circles (c, d) are uncorrected model results from case PAC. Stepped lines are satellite observations of line-shaped contrails over the eastern North Pacific (Minnis *et al.*, 2005). Curves with open circles are model results (c) using empirical detection efficiencies (see text) to adjust for undersampling of optically thin contrails in these observations and (d) using a single optical depth τ_{det}=0.04 above which the contrail radiative forcings are evaluated. Shading indicates undetectable optical depth and long-wave flux change values. The model distributions of the cloud-controlling factors, temperature and wind shear, were constrained by weather analysis data in the observation region and period, and sampled according to contrail width similar to the satellite observations. Otherwise, case PAC is identical to FULL. Constraining the model variability resulted in a mean temperature and standard deviation 224±3 K and mean wind shear 0.002 s^{-1}. Mean ice supersaturated layer depth is 1 km, mean RHI=115%, and T_b =280 K.

MIN, also include a few optically very thick contrails (τ=1 to 5) in the tails of their PDFs, inducing CRF values up to 100 W m^{-2}.

The CRFs (Figures 1(b, c)) include values of up to 40 W m^{-2} for the net CRF for contrail outbreaks as inferred from satellite observations (Duda *et al.*, 2001; Haywood *et al.*, 2009). The large variances of PDF(τ) (Figure 1(a)) result in large variances of the PDFs of net CRF (Figure 1(b)) and their SW and LW components (Figure 1(c)). Low (high) CRF values are associated with the low- (high-) τ end of PDF(τ). Figure 1(c) emphasizes that some contrails achieve very high SW and LW RFs in cases BASE, FULL, and MAX and that many more exist with low forcing values. Relatively high mean relative humidities over ice >115% and low mean shear values <0.004 s^{-1} are required to generate τ_m>0.2 and mean net CRF>10 W m^{-2}.

The average CRF values will be biased when optical depth variability is neglected, in particular when the optical depth approaches values (∼0.3−0.5) above which the deviation from linearity (CRF∝τ) becomes significant and the dispersion of PDF(τ), $\delta_\tau=\sigma_\tau/\tau_m$, is large ($\delta_\tau>1$). In such cases, the CRF biases are sensitive to the shape of PDF(τ). In Table 1 we compare CRFs evaluated at τ_m with those evaluated at different optical depths and then weighted by the corresponding PDF(τ) (describing variability around the same mean value). The relative CRF biases, Δ, in case FULL are almost as large as in MAX, despite a much smaller mean value, because δ_τ is very large. Biases are stronger in the LW than in the SW, as the emissivity depends exponentially on optical depth. The LW biases would be higher if the background brightness temperature was higher and mean contrail temperature was lower than assumed here. Both LW and SW biases are small in case MIN (< −5%) because τ_m is small. In all other cases, ignoring optical depth variability causes negative biases of −15% to −23% in average net CRFs. The LW bias in Pacific case study (PAC, see section 3.2.), compared with satellite observations below, is 21%.

Our results regarding the impact of the optical depth variability depend on how the data are sampled to compute PDF(τ). To generate the PDFs shown in Figure 1, we sampled the modelled contrails homogeneously, probing contrails filling a small volume as often as large ones, therefore giving each contrail the same weight irrespective of its dimension. In our cloud model, we keep the supersaturation and other contrail-controlling factors constant during the evolution of individual contrails. The contrail width depends on the contrail's vertical extent and the vertical wind shear; wide contrails are connected with high shear and low optical depth. This means that sampling contrails proportional to their width (and not homogeneously) would lead to a higher probability of optically thin contrails and therefore to smaller biases in cases MIN, MAX, BASE and FULL. On the other hand, it is not clear how effects not included in our cloud model would act to compensate this effect. Temperature and moisture variations (e.g. connected with gravity waves and moisture transport) would lead to a narrowing of PDF(τ) by dissipating particularly optically thin contrails or contrail areas in sublimation (warming) phases, whereas optically thicker contrails may survive the warming phase and gain ice water in the deposition (cooling) phase. In general, the optically thin portion of the PDF is likely more susceptible to changes, which would lead to a narrowing of the PDF.

Therefore, it is not clear how wide the PDF of optical depth would realistically be.

3.2. Comparison with satellite observations

We compare the statistics for young contrails (case PAC) obtained from the cloud model to the statistics from satellite observations of line-shaped contrails over the eastern North Pacific in the year 2001 (Minnis *et al.*, 2005) in Figure 2. The stepped lines in the bottom panels are annual average data derived from these regional observations. Average temperature and wind shear fields from numerical weather analyses over the observation region in 2001 were used to constrain the PDFs of contrail-controlling factors (see Figure 2 caption). We fixed $T_b = 280$ K in order to match the mean LW CRF from the observations.

In Figure 2 we make a detailed comparison with the satellite observations. In these observations, contrails were sampled weighted by their actual width, i.e. wider contrails were more frequently sampled than narrower ones. Therefore, we sampled contrail properties in the model case PAC weighted by their width, enabling us to compare realistically with the satellite data. Sampling in this way affects the PDF shapes and enhances the occurrence of optically thin contrails (K09).

The large variance of the simulated PDFs (Figures 2(a, b)) reflects the variety of meteorological conditions during an entire year of observations over the Pacific region. The larger skewness of the PDF of LW CRF as compared to PDF(τ) indicates that the linear relationship between LW CRF and τ no longer holds for optically thicker contrails ($\tau > 0.3$). We compare the PDFs with the observations that only include contrails up to $\tau = 1$ (Figures 2(c, d)). The observed PDFs show many fewer events at small τ and LW CRF values, because optically thinner contrails cannot be detected by the satellite. This undersampling is tied to lower limits on the contrail brightness temperature differences between two infrared channels in the satellite imagery. We adjusted the simulated PDF(τ) for the undersampling by deriving empirical detection efficiencies, $\epsilon(\tau)$, as described in K09. For the observations over the Pacific, we estimate $\epsilon = 11.5\%$ for data in the range $0 < \tau \leq 0.05$, 49% for $0.05 < \tau \leq 0.1$, 94.5% for $0.1 < \tau \leq 0.2$, and 100% for $\tau > 0.2$. Adjusting the simulated PDF(τ) with these efficiencies brings modelled and observed PDF(τ) in good agreement (Figure 2(c)). Together, the inferred ϵ values imply that the measurements detect only 39% of contrails over the whole range of optical depths. The same analysis of data taken over the USA yielded a similar result (K09).

Using the cumulative PDF(τ) for case PAC, we derive an ϵ-weighted detection threshold $\tau_{det} = 0.04$ below (above) which $\epsilon = 0$ ($\epsilon = 1$), as described in Kärcher *et al.* (2010). This threshold approximates the continuous detection efficiency curve by a step function, conserving the total fraction of undetected contrails (61%). The PDF of LW CRF (Figure 2(b)) indicates a high probability of low forcing values consistent with the low values of τ. Most optically thin contrails cannot be detected in the satellite images, because differences of infrared radiances between cloudy pixels and their surroundings become too small to be identified. Using $\tau_{det} = 0.04$ as a sharp cut-off, bounding the shaded area in Figure 2(a), improves the overall agreement between simulated and observed PDFs of LW CRF (Figure 2(d)). Remaining differences between observed and modelled (corrected for detection efficiency) PDFs are likely to be partly due to the approximation of the true synoptic situation and missing T_b variability in our model.

Inspection of PDF(τ) (Figure 2(a)) shows that 49% of all simulated contrails are subvisible ($\tau < 0.02$), up to 37% are visible but cannot (or can only partially) be detected ($0.02 \leq \tau \leq 0.2$), and 11% represent optically thicker cases ($\tau > 0.3$). We find that the cut-off optical depth value of 0.04 is associated with a cut-off of approximately 3 W m^{-2} for detection of LW radiance differences (bounding the shaded area in Figure 2(b)). Contrails inducing flux changes below this magnitude may exert a non-negligible climate impact, as our cloud simulations indicate that optically very thin, young contrails are very common and likely associated with large coverage (K09).

The model mean values of τ and LW CRF, computed from the PDFs shown in Figures 2(a, b), are 0.15 and 12.1 W m^{-2}, those from the observations are 0.24 and 14.2 W m^{-2} (Minnis *et al.*, 2005), i.e. mean τ and LW CRF have been overestimated in the observations by 60% and 17%, respectively. The measured values compare reasonably well with our model estimates, 0.29 for τ (ϵ-adjusted curve, Figure 2(c)) and 15.5 W m^{-2} for LW CRF (curve with cut-off at 0.04, Figure 2(d)) when excluding non-detectable clouds. We note that modelled (case PAC, including non-detectable contrails) and observed PDF variances are very different.

4. Conclusions

We conclude our study by summarizing the main results and by deducing implications for uncertainty estimates of the contrail cirrus climate impact.

4.1. Summary

The optical depth of contrails is highly variable, even within a specified region. Therefore, RF estimates based only on mean optical depth neglect important dynamical and microphysical information affecting mean radiative flux changes. We have quantified those for the first time for young contrails most likely comparable to, but including optically thin contrails not detected by, satellite observations of line-shaped contrails. We have found that optical depth variability has a non-negligible effect on contrail RF. It causes CRF biases of 10−20% which are of similar magnitude to effects caused by other factors determining the optical response of contrails, e.g. optical depth of low-level clouds or ground albedo, altitude or ice water content of contrails, ice crystal habit, or 3D effects (Meerkötter *et al.*, 1999; Gounou and Hogan, 2007; Yang *et al.*, 2010; Markowicz and Witek, 2011; Schumann *et al.*, 2011). We note that differences in the SW and LW CRF among various optical models–in which ice crystal radiative properties are treated by different methods–have been found to reach 44% and 23%, respectively, relative to the mean model value (Markowicz and Witek, 2011).

Our analysis has also yielded insight into the ability to infer CRF from space-borne passive remote sensing measurements. We have demonstrated that the mean optical depth and LW CRF in previous observations were overestimated by 60% and 17%, respectively, because optically thin contrails are not detected and are therefore not included in the averages. This undersampling is tied to the inability to detect regions of contrails with solar optical

depths below ≈0.04 and contrail-induced LW RF below ≈3 W m^{-2}, the exact values depending on the experimental detection efficiency and on the performance of the contrail model and the radiation parametrization. A similar effect on the SW flux changes is expected, but could not be evaluated here because the observations only provided LW data. We suggest that detection efficiencies should be better specified for both optical depth and radiative flux changes, e.g. by using multi-spectral satellite data with increased detection thresholds (Dessler and Yang, 2003).

4.2. Implications

The combination of calculated global contrail coverages which have been calibrated against regional satellite observations–with contrail optical depth detection thresholds that are not consistent with (independent from) these observations–has been shown to underestimate global contrail RF evaluated with GCMs relying on this scaling method (Kärcher *et al.*, 2010). The contribution to the global RF of line-shaped contrails that are not (or are only partially) detectable in satellite imagery ($\tau<0.05$) amounts to 36% according to GCM results (Frömming *et al.*, 2011). Therefore, omitting the non-detectable contrails would lead to a further underestimation of the global RF. Our present study suggests that disregarding microphysical optical depth variability leads to an overestimation of the total climate effect of line-shaped contrails. This conclusion would also carry forward to the evaluation of the total contrail cirrus climate impact.

We put the issue of the variability bias for contrails up for discussion and thereby raise an important aspect for the estimation of the contrail climate impact. The contrail optical depth variability discussed here affects radiative transfer calculations. RTMs neglecting this variability (i.e. when using constant optical depths) will overestimate CRF. Besides the need to use consistent datasets of contrail coverage and (mean) optical depth (Kärcher *et al.*, 2010), we suggest that RTMs should account for variability of optical depth as well. Spatial and temporal variability of contrail optical depth could be taken from detailed contrail simulations (e.g. those presented here) or from collocated space-borne lidar and infrared data (Iwabuchi *et al.*, 2012). As our findings are based on a simple radiative transfer parametrization, we recommend study of the effects of optical depth inhomogeneity on CRF using sophisticated RTMs which include effects of multiple scattering and horizontal photon transport. Furthermore, more work is needed to better characterize the underlying variability in the dynamical forcings and microphysical properties which ultimately determine the spatial and temporal contrail optical depth variability.

Appendix. Radiative flux changes

The radiative flux changes due to contrails have been calculated coupling a radiative transfer parametrization with microphysical contrail simulations. Contrary to previous studies which mostly relied on detailed RTMs combined with highly simplified assumptions regarding contrail microphysics, we use a simple approach to calculate radiative flux changes combined with a more detailed description of the contrail microphysical properties.

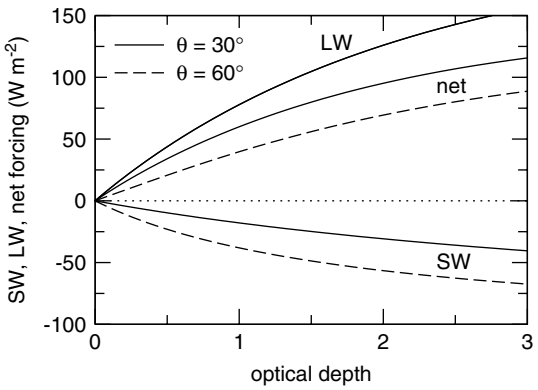

Figure A1. Short-wave, long-wave, and net flux changes due to contrails for two solar zenith angles (solid and dashed curves) as a function of contrail optical depth taken at solar wavelengths. The LW flux change does not depend on θ. Most contrails are optically thin, with mean values near 0.2; contrails with $\tau>3$ are very rare (Figure 1(a)).

We expect our equations used to estimate the SW and LW flux changes to be most accurate when applied to small optical depth values. The SW albedo change becomes inaccurate for large zenith angles. The LW emissivity, which includes a small scattering contribution, is accurate only at specific near-infrared wavelengths (6.5 μm and 10.5 μm). It is therefore necessary to assess whether our simple radiative transfer approach is suitable for estimating the effects of optical variability on CRF.

Optically thin contrails would not cause a CRF bias due to optical depth variability, because the respective CRF values scale linearly with optical depth. Therefore, the accuracy of our estimated CRF biases depends on the ability of the flux changes to capture the transition towards the nonlinear dependence in a range of medium optical depth values ($0.3<\tau<1$) where effects of multiple scattering become important. The behaviour of CRF(τ) in this transition region depends on the ice crystal optical model (Markowicz and Witek, 2011, their Figure 9).

Figure A.1 shows this transition region using g=0.8, A=0.2, θ=30°, T_b=280 K, and T_c=223 K. Our results compare favourably with those discussed for spherical ice crystals in Meerkötter *et al.* (1999, their Figure 3). A closer comparison with 1D RTM results is not straightforward since Meerkötter *et al.* (1999) employ spectral models, provide diurnal averages of the flux changes, and consider a specific vertical distribution of absorbing gases and clouds (determining T_b), while we apply a broadband model with fixed values for g and θ and do not resolve the atmosphere below and above the contrail layer. To estimate the accuracy of our parametrization, we have compared results for clear-sky midlatitude summer continental conditions (Meerkötter *et al.*, 1999, their Tables 4 and 5), using fixed values τ=0.52, θ = 30−60°, and T_b=288 K. Our individual flux changes in the SW and LW agree with the respective SW and LW estimates of Meerkötter *et al.* (1999) within 30%, with ΔF_{LW} being more accurate than ΔF_{SW}. It is possible that the agreement could be improved by systematically fitting the values of g, A, and T_b. More detailed radiative transfer schemes (Myhre *et al.*, 2009) show similarly large differences in CRF relative to each other when using fixed conditions for a number of parameters describing the atmosphere and contrail ice crystal single scattering properties.

Acknowledgements

We acknowledge fruitful discussions with David Fahey, Piers Forster, Patrick Minnis, and Michael Ponater. This work was performed within the DLR project 'Climate-compatible air transport system' and contributes to the 'Aviation Climate Change Research Initiative' organized by the US Federal Aviation Authority.

References

Burkhardt U, Kärcher B. 2009. Process-based simulation of contrail cirrus in a global climate model. *J. Geophys. Res.* **114**: D16201, DOI: 10.1029/2008JD011491

Burkhardt U, Kärcher B. 2011. Global radiative forcing from contrail cirrus. *Nature Climate Change* **1**: 54–58.

Charlson RJ, Schwartz SE, Hales JM, Coakley JA, Hansen JE, Hofmann DJ. 1992. Climate forcing by anthropogenic aerosols. *Science* **255**: 423–430.

Coakley JA, Chylek P. 1975. The two-stream approximation in radiative transfer: Including the angle of the incident radiation. *J. Atmos. Sci.* **32**: 409–418.

Dessler AE, Yang P. 2003. The distribution of tropical thin cirrus clouds inferred from Terra MODIS data. *J. Climate* **16**: 1241–1247.

Duda DP, Minnis P, Nguyen L. 2001. Estimates of cloud radiative forcing in contrail clusters using GOES imagery. *J. Geophys. Res.* **106**: 4927–4937.

Fahey DW, Schumann U. 1999. Aviation-produced aerosols and cloudiness. In *Aviation and the Global Atmosphere: The Physical Science Basis: A special report of IPCC Working Groups I and III*. Penner JE, Lister DH, Griggs DJ, Dokken DJ, McFarland M (eds), Cambridge University Press: Cambridge, UK, and New York.

Febvre G, Gayet J-F, Minikin A, Schlager H, Shcherbakov V, Jourdan O, Busen R, Fiebig M, Kärcher B, Schumann U. 2009. On optical and microphysical characteristics of contrails and cirrus. *J. Geophys. Res.* **114**: D02204, DOI: 10.1029/2008JD010184

Frömming C, Ponater M, Burkhardt U, Stenke A, Pechtl S, Sausen R. 2011. Sensitivity of contrail coverage and contrail radiative forcing to selected key parameters. *Atmos. Env.* **45**: 1483–1490.

Gounou A, Hogan RJ. 2007. A sensitivity study of the effect of horizontal photon transport on the radiative forcing of contrails. *J. Atmos. Sci.* **64**: 1706–1716.

Haywood JM, Allan RP, Bornemann J, Forster PM, Francis PN, Milton S, Rädel G, Rap A, Shine KP, Thorpe R. 2009. A case study of the radiative forcing of persistent contrails evolving into contrail-induced cirrus. *J. Geophys. Res.* **114**: D24201, DOI: 10.1029/2009JD012650

Heymsfield A, Baumgardner D, DeMott P, Forster PM, Gierens K, Kärcher B. 2010. Contrail microphysics. *Bull. Am. Meteorol. Soc.* **91**: 465–472.

Iwabuchi H, Yang P, Liou KN, Minnis P. 2012. Physical and optical properties of persistent contrails: Climatology and interpretation. *J. Geophys. Res.* **117**: D24201, DOI: 10.1029/2011JD017020

Kärcher B, Burkhardt U, Unterstrasser S, Minnis P. 2009. Factors controlling contrail cirrus optical depth. *Atmos. Chem. Phys.* **9**: 6229–6254.

Kärcher B, Burkhardt U, Ponater M, Frömming C. 2010. Importance of representing optical depth variability for estimates of global line-shaped contrail radiative forcing. *Proc. Nat. Acad. Sci. USA* **107**: 19181–19184.

Liou KN, Ou SC, Takano Y, Valero FPJ, Ackerman TP. 1990. Remote sounding of the tropical cirrus cloud temperature and optical depth using 6.5 and 10.5 μm radiometers during STEP. *J. Appl. Meteorol.* **29**: 716–726.

Markowicz K, Witek M. 2011. Simulations of contrail optical properties and radiative forcing for various crystal shapes. *J. Appl. Meteorol. Climatol.* **50**: 1740–1755.

Meerkötter R, Schumann U, Doelling DR, Minnis P, Nakajima T, Tsushima Y. 1999. Radiative forcing by contrails. *Ann. Geophys.* **17**: 1080–1094.

Minnis P, Palikonda R, Walter BJ, Ayers JK, Mannstein H. 2005. Contrail properties over the eastern North Pacific from AVHRR data. *Meteorol. Z.* **14**: 515–523.

Myhre G, Kvalevåg M, Rädel G, Cook J, Shine KP, Clark H, Karcher F, Markowicz K, Kardas A, Wolkenberg P, Balkanski Y, Ponater M, Forster PM, Rap A, de Leon RR. 2009. Intercomparison of radiative forcing calculations of stratospheric water vapour and contrails. *Meteorol. Z.* **18**: 585–596.

Rockel B, Raschke E, Weyres B. 1991. A parametrization of broad band radiative transfer properties of water, ice, and mixed clouds. *Beitr. Phys. Atmos.* **64**: 1–12.

Schumann U, Mayer B, Gierens K, Unterstrasser S, Jessberger P, Petzold A, Voigt C, Gayet J-F. 2011. Effective radius of ice particles in cirrus and contrails. *J. Atmos. Sci.* **68**: 300–321.

Twomey S. 1977. *Atmospheric Aerosols. Development in Atmospheric Science* 7. Elsevier/North-Holland: Amsterdam.

Yang P, Hong G, Dessler AE, Ou SC, Liou KN, Minnis P, Hashvardhan. 2010. Contrails and induced cirrus: Optics and radiation. *Bull. Am. Meteorol. Soc.* **91**: 473–478.

